33RD CONGRESS
OF THE INTERNATIONAL COUNCIL
OF THE AERONAUTICAL SCIENCES
STOCKHOLM, SWEDEN, 4-9 SEPTEMBER, 2022

ICAS 2022 SWEDEN

PARAMETER IDENTIFICATION BY UPDATING THE STRUCTURAL MODEL OF A UAV WITH FLEXIBLE WING

Thiago Rosado de Paula[1], Vitor Paixão Fernandes[1], Andrew Gomes Pereira Sarmento[1], David Fernando Castillo Zuñiga[1], Alain Giacobini Souza[2], Roberto Gil Annes da Silva[1] & Luiz Carlos Sandoval Góes[1]

[1]Aeronautics Institute of Technology
[2]Universidade de Lisboa

Abstract

There are some approaches for updating models to later model the aeroelastic behavior, and in this work, the Modal Assurance Criterion (MAC) helps identify the parameters. The objective of this work was to update the finite element model for the EOLO aircraft. We used the modal shapes derived from Ground Test Vibration (GVT) as a basis of comparison for the MAC, in addition to using the Nastran software to optimize the stiffness properties of the analytical model of the EOLO aircraft. It noted that the natural frequencies of the updated model approached the GVT data and the cross-correlation improved, but the correlation was far from ideal. Therefore, the model was updated and improved over the initial model.

Keywords: MAC, GVT, Structural model, Natural frequencies, Finite Element Method.

1. Introduction

Carrying out the modeling and simulation of the flight mechanics of flexible aircraft depends on developing coupled aerodynamic and structural models. The mechanical flight described not-linearly can be derived based on finite element models and aerodynamic theory, for example, lift surface theory, Vortex-Lattice Method (VLM) Doublet-Lattice Method, ZONA6, among others. Indeed, accurate flight mechanics prediction is highly dependent on the accuracy of these structural models and aerodynamic [5].

The accuracy of the structural model, in particular the stiffness characteristics, based on the theoretical model is not reliable enough. Because of this, airworthiness regulations require those aircraft structural models used for aeroelastic calculations or flight mechanics of flexible aircraft to be certified through experimental results. Ground vibration testing (GVT) is one of the most critical experiments during aircraft development. The primary input data for the flutter analysis are the aircraft's modal shapes, results from the GVT or Finite Element Method [9, 8].

There are two approaches concerning the GVT of how to input the results into the analysis. Direct use of GVT results for analysis is the first choice. An advantage and a disadvantage are, respectively, the direct relationship of the modal shape with the actual structure of the aircraft, and the analyzes are more or less limited to the tested structure [9].

The second option is to update an aircraft structure model to GVT results before analysis. The analytical model, usually based on the Finite Element Method (FEM), is updated to match the modal shapes of the GVT as closely as possible. The relationship with the real object of study is indirect. The advantage of the updated model is that it allows for parametric studies and modifications of structural parameters and changes [9].

System identification is the field in which researchers are dedicated to developing modeling methods inspired by obtaining experimental data to reduce the difference in the problem's analytical model. The model must be identified non-parametrically or parametrically. For the parametric identification

of structural dynamics, the experimental modal analysis must be considered a special field for determining modal analysis data [6, 7].
In the literature, it is common to find numerous methods to increase the accuracy of numerical/analytical structural models in relation to the experimental results, updating the model parameters[5]. There are several methods for updating models, such as the Modal Assurance Criterion (MAC), which uses modal shapes data from two sources to assess the correlation between these two data sources. It is usual to use data from the Ground Vibration Test (GVT) mode shapes concerning the mode shapes from the analytic/numerical models [7].
This work aims to update the EOLO aircraft's finite element model, identifying properties for each beam using MAC to assess whether the estimated parameters have been improved.

2. Modal Analysis

This work used the EOLO aircraft with flexible wings from the Aeronautical Systems Laboratory (LSA) of the Aeronautics Institute of Technology (ITA). Figure 1 shows the aircraft model, and Table 1 presents the values of some geometric and mass properties.

Figure 1 – EOLO aircraft [3].

Table 1 – Mass and geometry parameters [4]

Parameters	Values
Wing area	0.846 m²
Wing span	4.00 m
Aspect Ratio	18.9
Wing mass	2 kg
Total mass	8.87 kg
X moment of inertia	2.53 kg m²
Y moment of inertia	1.60 kg m²
Z moment of inertia	3.96 kg m²

For the simulations, the structural model of a beam was used to represent the structural model. To make the model, it started with the complete aircraft model, as seen in Figure 2. Rigid bar elements were also used to characterize the ends of each member of the aircraft, as seen in Figure 3. Table 2 presents the basic configurations present in the aircraft model.

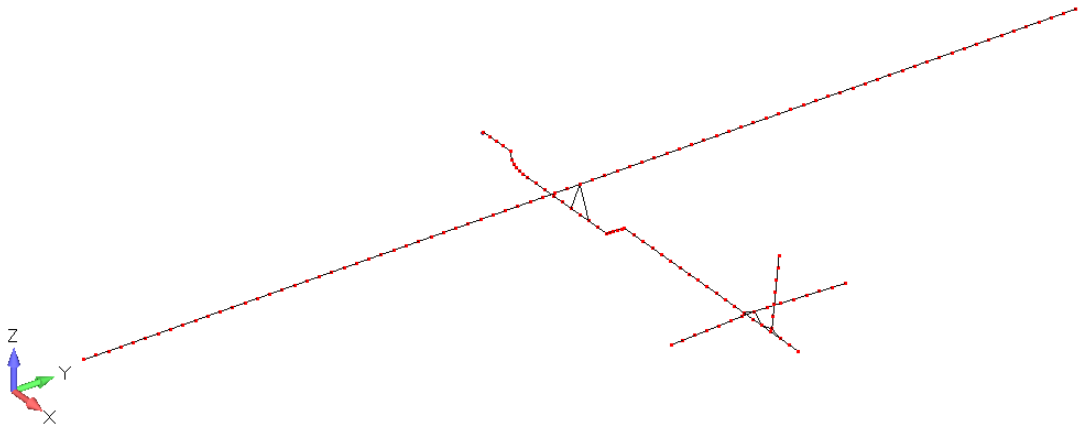

Figure 2 – EOLO Beam Model.

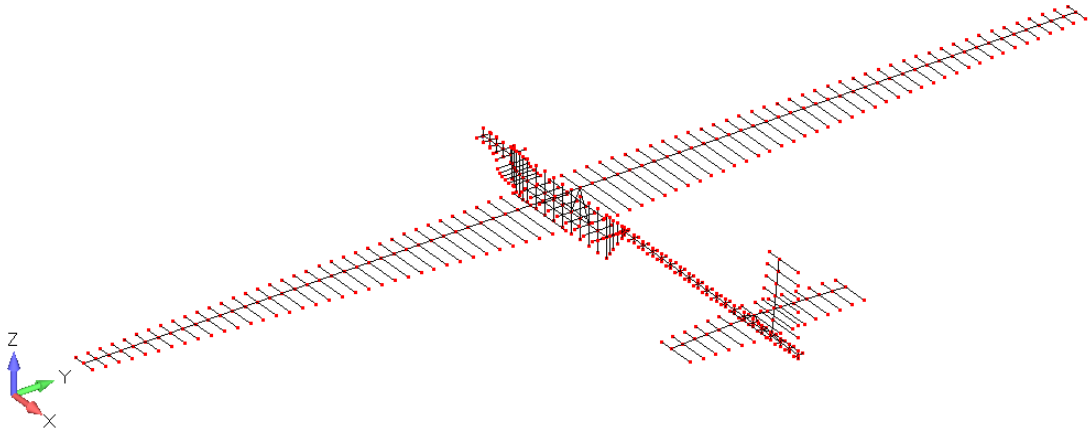

Figure 3 – EOLO Beam Model with rigid bar elements.

Table 2 – Basic properties of the aircraft finite element model.

Properties	Values
Fuselage Nodes	44
Fuselage Elements	43
Wing Nodes	81
Wing Elements	80
Horizontal Tail Nodes	15
Horizontal Tail Elements	14
Vertical Tail Nodes	7
Vertical Tail Elements	6

2.1 Modal shapes from GVT

For this work, data from tests developed by [3] were used, in which the behavior of the first eight vibration modes are presented in raw form and with interpolation in Figures 4, 5, 6 and 7. The modal shapes were obtained through Experimental Modal Analysis (EMA). The first modal shape is the first

bending symmetrical mode of the wing. The first mode has the wing as its main contributing component. There is no significant contribution from torsion of the fuselage in this mode. The second modal shape has the main contribution from tail-boom torsion. One is noted that in this mode, the wing contributes anti-symmetrical wingtip bending and slight torsion. The third and fourth modal shapes have similar characteristics. Both have the main characteristic of anti-symmetrical wing bending. The difference between the two modes is that the tail-boom twist is in phase with the central chord of the wing. The fifth mode is a symmetrical wing twist. In this mode, there is the contribution of tail-boom bending. The sixth vibration mode is the first anti-symmetrical wing torsion mode. The seventh mode of vibration is the second symmetrical wing torsion mode. The symmetrical wing twist participates in this mode as well. The eighth mode of vibration is the second anti-symmetrical mode of wing flexion. In Table 3, one can see, in summary, the natural frequencies and damping for each mode.

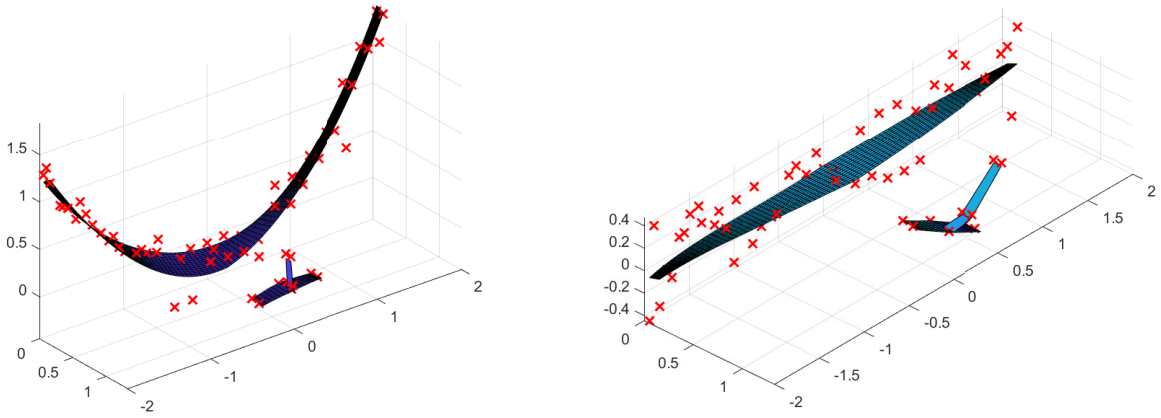

(a) Shape of the first mode from GVT.

(b) Shape of the second mode from GVT.

Figure 4 – Behavior of the first and second modes from GVT.

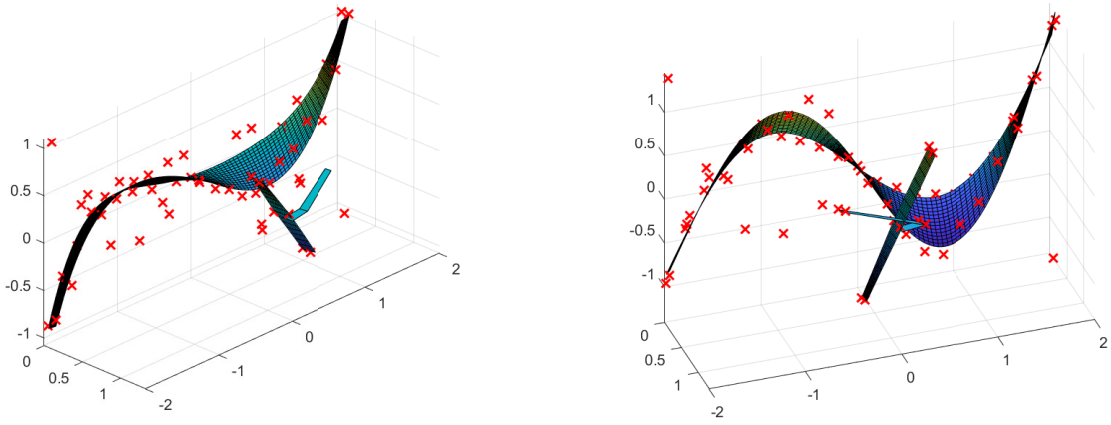

(a) Shape of the third mode from GVT.

(b) Shape of the fourth mode from GVT.

Figure 5 – Behavior of the third and fourth modes from GVT.

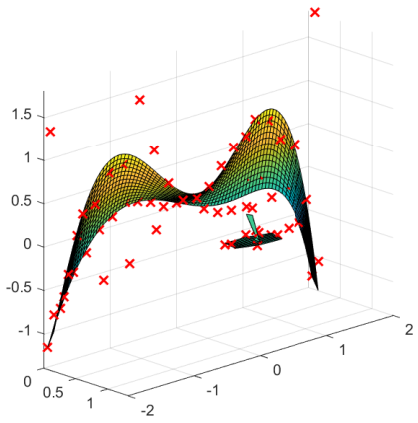

(a) Shape of the fifth mode from GVT.

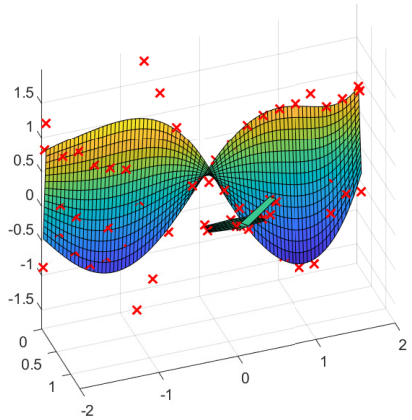

(b) Shape of the sixth mode from GVT.

Figure 6 – Behavior of the fiveth and sixth modes from GVT.

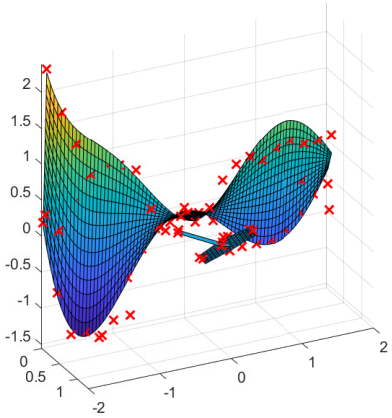

(a) Shape of the seventh mode from GVT.

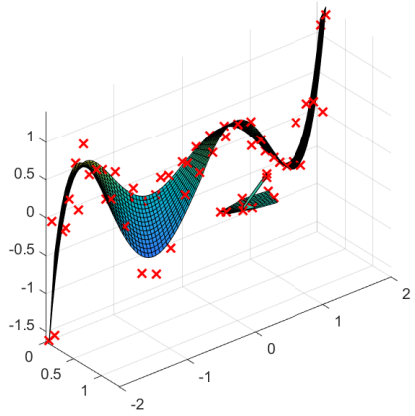

(b) Shape of the eighth mode from GVT.

Figure 7 – Behavior of the seventh and eighth modes from GVT.

Table 3 – Natural frequencies and damping for each mode [3]

Mode	Frequency [Hz]	Damping
1st Symmetrical wing bending	4.4277	1.6
Tail-boom torsion	7.6076	2.1
1st Anti-symmetrical wing bending + tail-boom torsion	10.5233	2.2
1st Anti-symmetrical wing bending + tail-boom torsion	11.6088	1.2
1st Symmetrical wing torsion + tail-boom bending	14.9733	1.7
1st Anti-symmetrical wing torsion	19.0827	3.2
2nd Symmetrical wing bending + symmetrical wing torsion	21.1676	3.8
2nd Anti-symmetrical wing bending	30.3827	2.4

2.2 Modal Assurance Criterion

The metric MAC was used, which is, in the literature, a standard metric to assess the modes shape [5], and measures the correlation from the modes shapes between two different data sources for the same case. MAC is defined according to Equation 1.

$$MAC(\phi_{id,i}, \phi_{fe,i}) = \frac{|\phi_{id,i}^T \phi_{fe,i}|^2}{\phi_{id,i}^T \phi_{id,i} \phi_{fe,i}^T \phi_{fe,i}} \quad (1)$$

Where $\phi_{id,i}$ and $\phi_{fe,i}$ are the i-th modal vector of the first source and second source, respectively, the MAC value can range between 0 and 1, where 1 means the modal vectors from two sources are consistent.

3. Finite Element Optimization

It is necessary to bring the MAC value, between the GVT and the Finite Element model, for each mode shape closer to 1. In addition to approximating the modal forms, it is necessary to reduce the difference between the modal frequencies calculated through the element model finite and the GVT. Initially, the mass properties in Table 1 were used to adjust the mass properties of the finite element model of the aircraft shown in Figure 3 and Table 2. Concentrated masses were used to distribute and adjust the model properties. With the updated structural model with masses of the aircraft, the Equation 2 was used to optimize the FEM [1].

$$f = \sum_{i=1}^{n} \left[[1 - MAC(\phi_{id,i}, \phi_{fe,i})] + \left(\frac{\omega_{id,i} - \omega_{fe,i}}{\omega_{id,i}} \right)^2 \right] \quad (2)$$

Which, n is the number of identified modes, $\omega_{id,i}$ e $\omega_{fe,i}$ are the i-th mode shape of the GVT and finite element model, respectively.

To optimize the Equation 2, Matlab was used to generate Nastran files and design sensitivity analysis in Nastran to optimize the cost function. The nastran files ware run on MSC Nastran. As the GVT data is mainly for the wing, horizontal stabilizer, and vertical stabilizer, in addition to the wing properties, only the tail properties were optimized in order to simplify the search for the optimized model. Table 4 shows that the first two lines are properties searched for tail-boom. The next ten lines are the wing properties, while the last four are the properties for the horizontal stabilizer, the vertical stabilizer, fuselage wing connection, and fuselage stabilizer connection, respectively. It was considered an isotropic material to complete aircraft. It has been observed that the X moments of inertia and torsional constant were varied for each property.

Table 4 – Initial conditions of the aircraft model and range of values for optimization.

	I_{xx} [m^4]			J [m^4]		
	Lower limit	**Initial value**	**Upper limit**	**Lower limit**	**Initial value**	**Upper limit**
Prop. 1	1.0E-11	3.680E-08	5.0E-01	1.0E-11	7.370E-08	5.0E-01
Prop. 2	1.0E-11	3.680E-08	5.0E-01	1.0E-11	7.370E-08	5.0E-01
Prop. 3	5.0E-11	6.600E-07	1.0E-04	5.0E-11	5.010E-07	9.0E-04
Prop. 4	5.0E-11	5.527E-07	1.0E-04	5.0E-11	4.142E-07	9.0E-04
Prop. 5	5.0E-11	4.585E-07	1.0E-04	5.0E-11	3.384E-07	9.0E-04
Prop. 5	5.0E-11	3.762E-07	1.0E-04	5.0E-11	2.726E-07	9.0E-04
Prop. 7	5.0E-11	3.048E-07	1.0E-04	5.0E-11	2.160E-07	9.0E-04
Prop. 8	5.0E-11	2.434E-07	1.0E-04	5.0E-11	1.678E-07	9.0E-04
Prop. 9	5.0E-11	1.910E-07	1.0E-04	5.0E-11	1.270E-07	9.0E-04
Prop. 10	5.0E-11	1.468E-07	1.0E-04	5.0E-11	9.300E-08	9.0E-04
Prop. 11	5.0E-11	1.099E-07	1.0E-04	5.0E-11	6.500E-08	9.0E-04
Prop. 12	5.0E-11	7.950E-08	1.0E-04	5.0E-11	4.240E-08	9.0E-04
Prop. 13	5.0E-11	1.333E-07	1.0E-04	5.0E-11	9.970E-08	9.0E-04
Prop. 14	5.0E-11	1.333E-07	1.0E-04	5.0E-11	9.970E-08	9.0E-04
Prop. 15	5.0E-11	4.570E-07	1.0E-01	5.0E-11	9.141E-07	1.0E-01
Prop. 16	5.0E-11	4.570E-07	1.0E-01	5.0E-11	9.141E-07	1.0E-01

4. Results

In this section, the complete aircraft's mass distribution showed. Then, stiffness properties and frequency results are presented for the aircraft considering isotropic materials. Subsequently, the modal shapes for the complete aircraft were presented for both the initial and the updated model. Finally, the results obtained through the MAC were presented.

4.1 Optimization

4.1.1 Aircraft mass distribution

In order to reach the mass parameters presented in Table 1, concentrated masses distributed throughout the aircraft were used. In this way, the mass distribution can be observed in Figure 8 and, in Table 5, the comparison between the measured mass parameters and that obtained in the model of Figure 8 can be observed. From Table 5, it can be seen that the errors between the measured values and those obtained from the finite element model are less or equal than 2.0%.

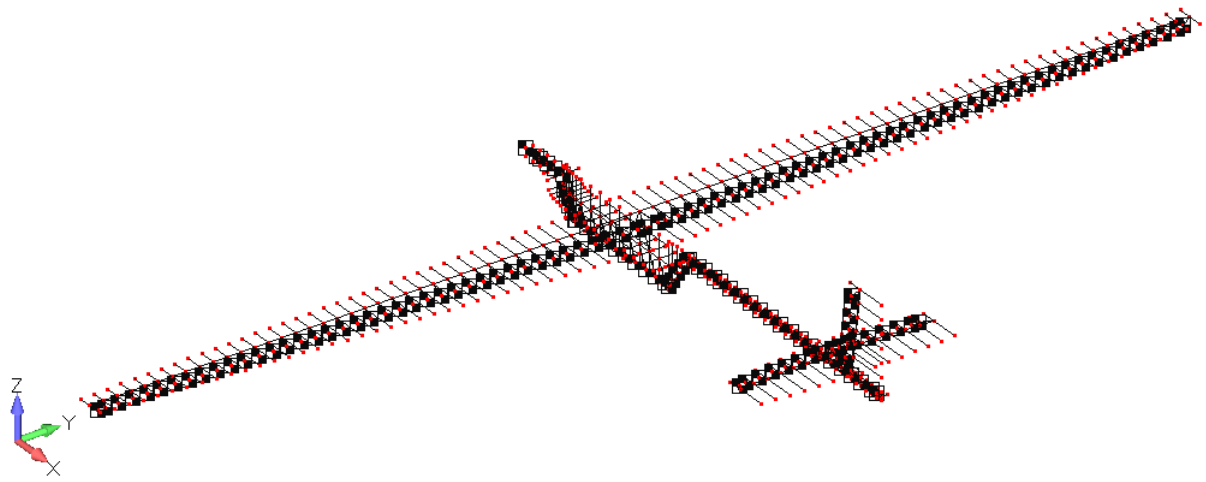

Figure 8 – EOLO mass distribution.

Table 5 – Mass parameters.

Parameters	Measured	FEM	Error [%]
Wing mass	2 kg	2 kg	0
Total mass	8.87 kg	8.8704 kg	0.005
X moment of inertia	2.53 kg m²	2.53736 kg m²	0.29
Y moment of inertia	1.60 kg m²	1.567972 kg m²	2.00
Z moment of inertia	3.96 kg m²	3.977671 kg m²	0.54

4.1.2 Aircraft optimization

After the simulations, it arrived at Tables 6 and 7 resulting from the aircraft updated. Table 6 demonstrates that the natural aircraft frequencies after updated approached the GVT frequencies [2]. After the updated, multiplying the properties of the materials with the section's properties, the final values for the bending and torsional stiffness for each section were arrived at, as shown in Table 7.

Table 6 – Aircraft natural frequencies for each mode.

	FEM (Hz)	Updated FEM (Hz)	GVT (Hz)
First mode	2.1069	4.5583	4.4277
Second mode	5.8887	7.3160	7.6076
Third mode	9.6005	10.4801	10.5233
Fourth mode	14.0249	10.8713	11.6088
Fifth mode	18.6738	13.1592	14.9733
Sixth mode	23.5311	17.6960	19.0827
Seventh mode	26.3876	25.7764	21.1676
Eighth mode	30.0965	26.6523	30.3827

Table 7 – Stiffness properties initial and final for each aircraft property.

Bending [$N \cdot m^2$]	**Initial value**	**Final value**	**Torsional [$N \cdot m^2$]**	**Initial value**	**Final Value**
$EI_{xx,1}$	2.0070E+03	7.4500E+02	GJ_1	2.6770E+03	2.4800E+03
$EI_{xx,2}$	1.6590E+03	3.9500E+02	GJ_2	2.5520E+03	7.0000E+01
$EI_{xx,3}$	1.2500E+02	3.3200E+02	GJ_3	8.6000E+01	2.4000E+01
$EI_{xx,4}$	1.0400E+02	3.6900E+02	GJ_4	7.1000E+01	2.5000E+01
$EI_{xx,5}$	8.7000E+01	2.1800E+02	GJ_5	5.8000E+01	3.2000E+01
$EI_{xx,6}$	7.1000E+01	1.4200E+02	GJ_6	4.7000E+01	3.9000E+01
$EI_{xx,7}$	5.8000E+01	1.7800E+02	GJ_7	3.7000E+01	4.1000E+01
$EI_{xx,8}$	4.6000E+01	1.8400E+02	GJ_8	2.9000E+01	3.6000E+01
$EI_{xx,9}$	3.6000E+01	1.1000E+02	GJ_9	2.2000E+01	2.7000E+01
$EI_{xx,10}$	2.8000E+01	3.3000E+01	GJ_{10}	1.6000E+01	1.8000E+01
$EI_{xx,11}$	2.1000E+01	7.0000E+00	GJ_{11}	1.1000E+01	1.2000E+01
$EI_{xx,12}$	1.5000E+01	1.3000E+01	GJ_{12}	7.0000E+00	7.0000E+00
$EI_{xx,13}$	4.0000E+03	3.9680E+03	GJ_{13}	2.7200E+03	2.7160E+03
$EI_{xx,14}$	4.0000E+03	3.9920E+03	GJ_{14}	2.7200E+03	2.7190E+03
$EI_{xx,15}$	4.1134E+04	4.0828E+04	GJ_{15}	6.1394E+04	6.1338E+04
$EI_{xx,16}$	4.1134E+04	4.1045E+04	GJ_{16}	6.1394E+04	6.1150E+04

4.2 Mode Shapes

The aircraft model update allowed the natural frequencies to approach the GVT modes and the modal shapes improved compared to the initial ones; however, some modal forms did not achieve satisfactory results, observing the MAC values.

In Figures 9a, 10a, 11a, 12a, 13a, 14a, 15a and 16a the first eight aircraft mode shapes are presented according to the acquired of the initial finite element model. Figures 9b, 10b, 11b, 12b, 13b, 14b, 15b and 16b the first eight aircraft mode shapes are presented according to the acquired of the updated finite element model.

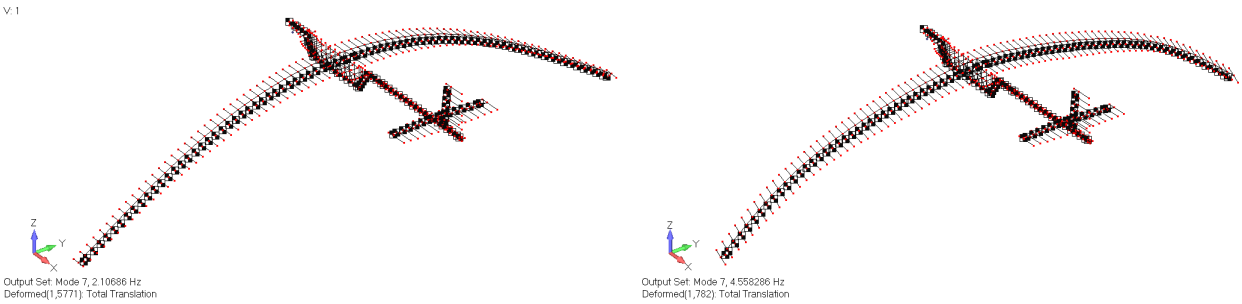

(a) Initial Finite Element Model. (b) Updated Finite Element Model.

Figure 9 – Behavior comparison between original FEM and updated FEM for the first mode.

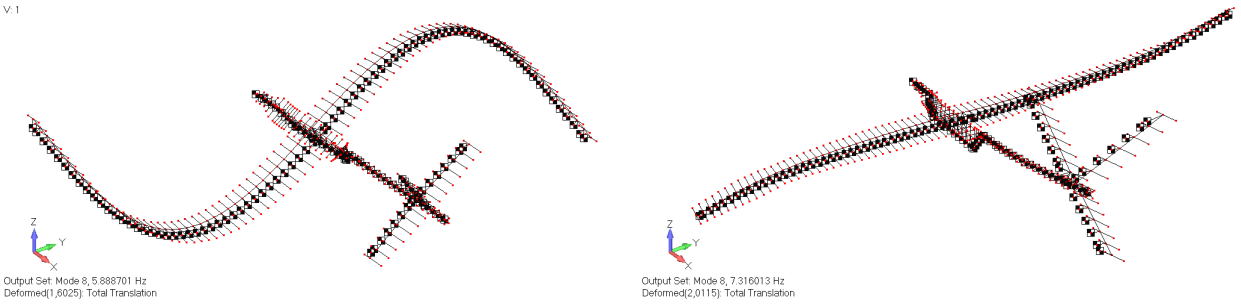

(a) Initial Finite Element Model. (b) Updated Finite Element Model.

Figure 10 – Behavior comparison between original FEM and updated FEM for the second mode.

(a) Initial Finite Element Model. (b) Updated Finite Element Model.

Figure 11 – Behavior comparison between original FEM and updated FEM for the third mode.

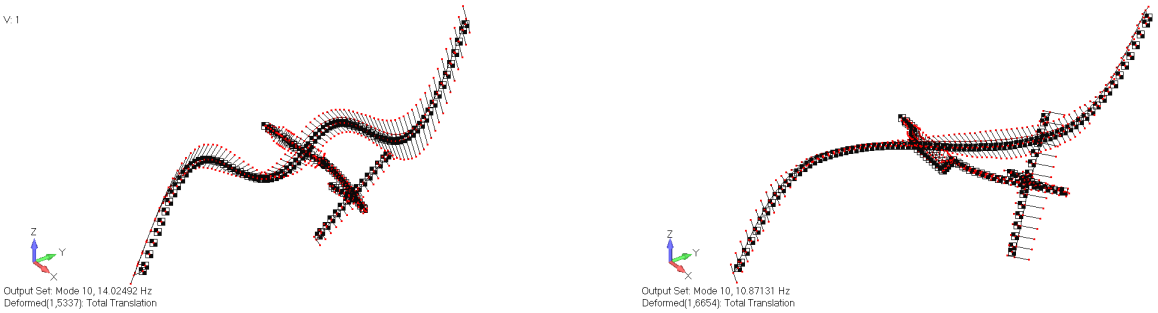

(a) Initial Finite Element Model. (b) Updated Finite Element Model.

Figure 12 – Behavior comparison between original FEM and updated FEM for the fourth mode.

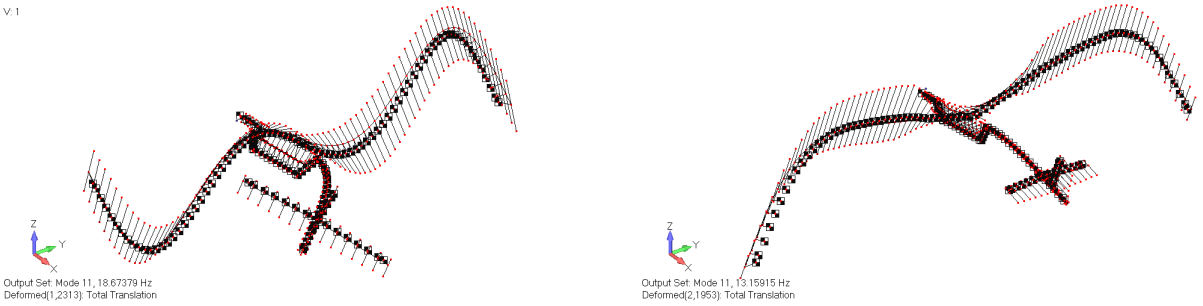

(a) Initial Finite Element Model. (b) Updated Finite Element Model.

Figure 13 – Behavior comparison between original FEM and updated FEM for the fifth mode.

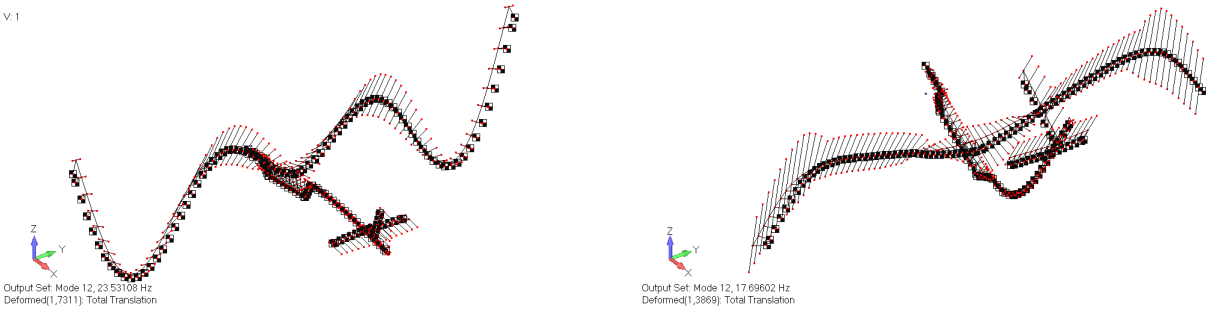

(a) Initial Finite Element Model. (b) Updated Finite Element Model.

Figure 14 – Behavior comparison between original FEM and updated FEM for the sixth mode.

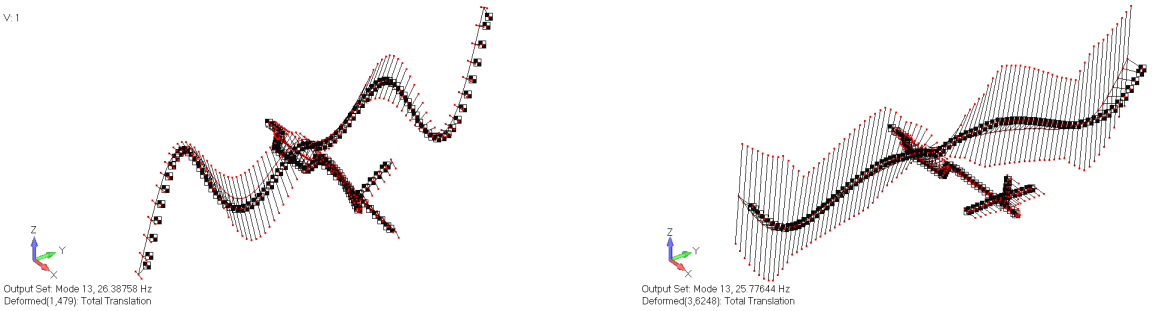

(a) Initial Finite Element Model. (b) Updated Finite Element Model.

Figure 15 – Behavior comparison between original FEM and updated FEM for the seventh mode.

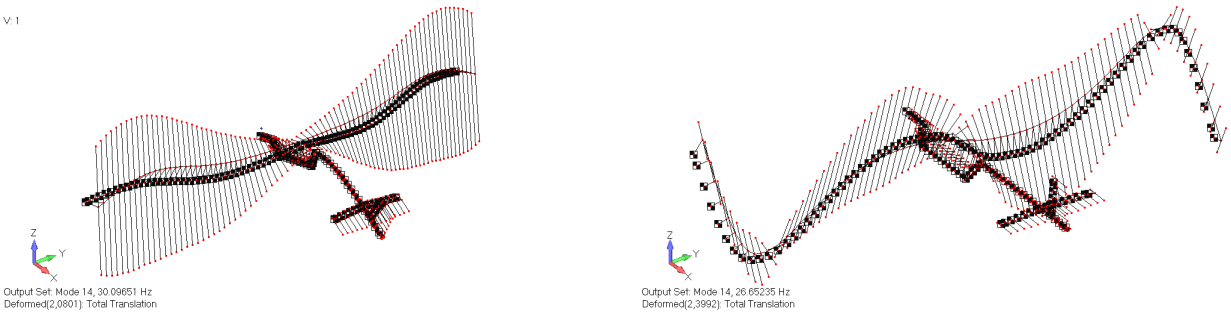

(a) Initial Finite Element Model. (b) Updated Finite Element Model.

Figure 16 – Behavior comparison between original FEM and updated FEM for the eighth.

It is possible to verify that there was an approximation of the displacement values of the updated FEM about the GVT in all the studied modes about the initial FEM. However, as shown in Figures 14b and 16b and Table 6, the approach after the update was still not enough and still needed to be improved to improve some modes, such as, for example, the sixth mode.

4.3 Modal Assurance Criterion Results

Using Equation 1, it was found cross-correlation values between the initial FEM and updated FEM shown Figure 17. In Table 8 it is possible to observe the MAC main diagonal values.

Table 8 – MAC main diagonal between initial FEM and Updated FEM.

	MAC value
First mode	0.9893
Second mode	0.3122
Third mode	0.0000
Fourth mode	0.5381
Fifth mode	0.0000
Sixth mode	0.0287
Seventh mode	0.0000
Eighth mode	0.0000

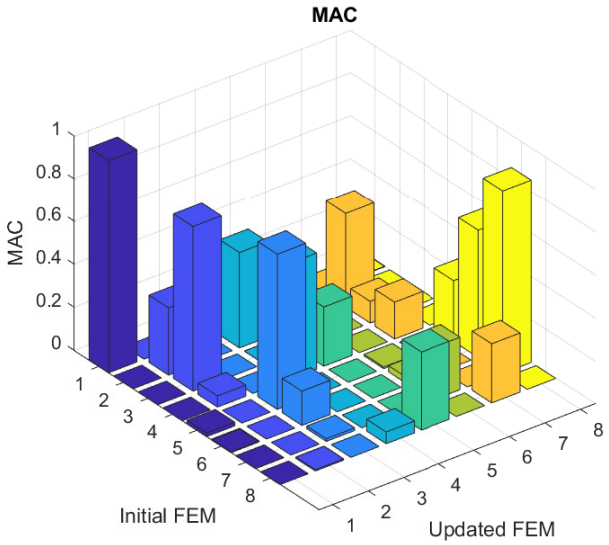

Figure 17 – MAC initial FEM and Updated FEM.

It was observed on the MAC main diagonal that the autocorrelation is close to one only first element. The initial FEM has a low cross-correlation with the updated FEM. This demonstrates, together with Figures 9, 10, 11, 12, 13, 14, 15 and 16 that the nodal displacements for both the initial FEM and the updated FEM have different values.
Related to what was seen above, the values of the cross-correlation between the initial FEM and the GVT were found in Table 9 and Figure 18.

Table 9 – MAC main diagonal between initial FEM and GVT.

	MAC value
First mode	0.9527
Second mode	0.2463
Third mode	0.0021
Fourth mode	0.4245
Fifth mode	0.0039
Sixth mode	0.0079
Seventh mode	0.0162
Eighth mode	0.0000

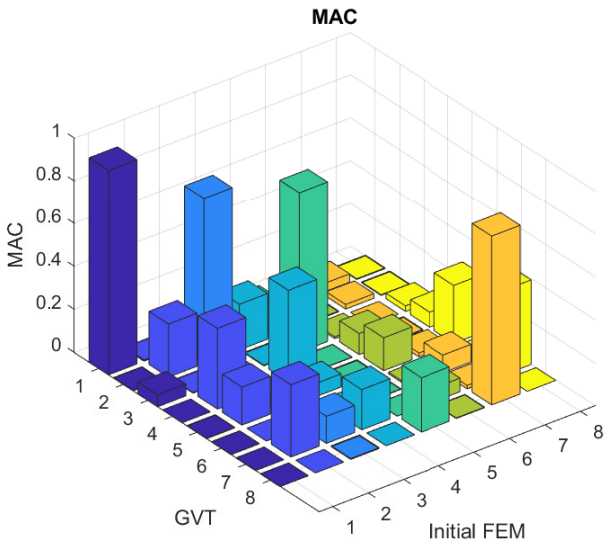

Figure 18 – MAC initial FEM and GVT.

On the main diagonal of the MAC autocorrelation, it can be seen that the first element approaches 0.9 in the first term. However, the other elements have a value lower than 0.45 on the main diagonal. In addition, they have a term off the main diagonal with a correlation close to 0.8; that is, the initial FEM does not have high cross-correlation with the GVT. This demonstrates, together with Figures 9a, 10a, 11a, 12a, 13a, 14a, 15a and 16a, that the nodal displacements for the initial FEM are far from the GVT values.
Similar to the above, the cross-correlation values between the updated FEM and the GVT were shown in Table 10 and Figure 19.

Table 10 – MAC main diagonal between Updated FEM and GVT.

	MAC value
First mode	0.9453
Second mode	0.8318
Third mode	0.8341
Fourth mode	0.7368
Fifth mode	0.9279
Sixth mode	0.0002
Seventh mode	0.7046
Eighth mode	0.6238

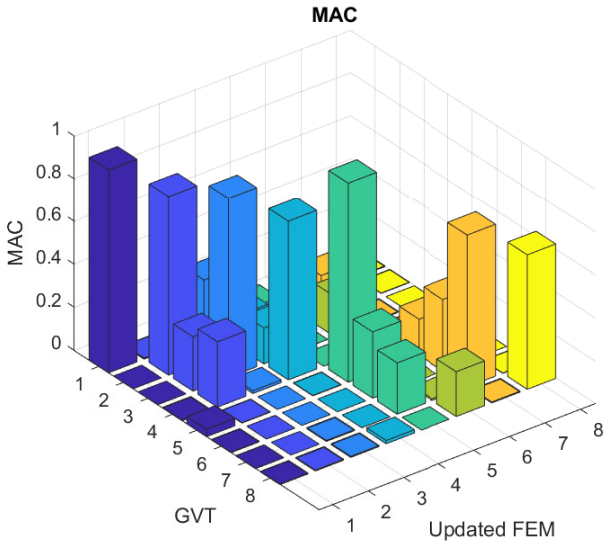

Figure 19 – MAC updated FEM and GVT.

On the main diagonal of the MAC autocorrelation, one can see that the first, second, third, fourth, fifth, and seventh elements have a value greater than 0.7. However, the sixth and eighth elements have a value smaller than 0.65 and, in addition, the terms off the main diagonal with a correlation lower than 0.4; that is, the updated FEM has significant cross-correlation with the GVT. However, it is noted that after the update, the elements of the main diagonal and the term off the main diagonal increased the accuracy concerning what was observed for the cross-correlation of the initial FEM and the GVT. This proves, together with Figures 9b, 10b, 11b, 12b, 13b, 14b, 15b and 16b, that the nodal offsets for the updated FEM are different from the GVT values, but are better than the initial FEM in relation to the GVT.

These results demonstrate that the known initial values of the properties give results that are not consistent with experimental results. Furthermore, it is necessary to adopt initial conditions that improve the search to improve the optimization results. In addition, to optimize fuselage properties, consideration should be given to collecting fuselage acceleration data during GVT.

Similar to what was seen before, the values of the GVT autocorrelation were shown in Figure 20.

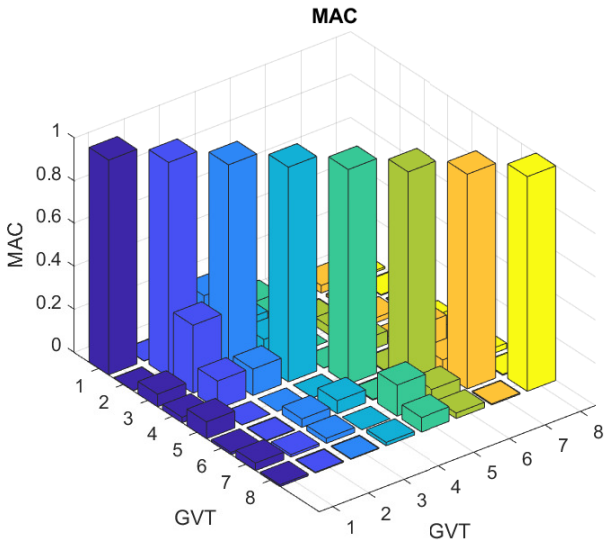

Figure 20 – GVT autocorrelation for the first bending modes.

In Figure 20, there are some values on the secondary diagonal with values greater than 0.5, demonstrating that the first mode is not entirely pure.

5. Conclusion and Future Works

After optimization, each mode's frequencies approximated the aircraft's GVT data.
It was verified that the MAC of the optimization FEM and original simulation in FEM obtained a low correlation in the main diagonal. That demonstrates that the known properties initially did not produce results consistent with experimental data.
The MAC of FEM optimization obtained a correlation higher than 0.7 in most modes. Nevertheless, the sixth and eighth modes had MAC lower than 0.65. In addition, the main diagonal terms had values less than 0.4. That demonstrated that optimization improved the results, but it can be enhanced to all modes to get close to 1.
Therefore, to improve the update, it is necessary to use a broader range of values for the material properties or section properties or use a heuristic method to aid in the search. Furthermore, for future work, two-dimensional elements can be used to insert different properties of the materials and improve the results.

6. Acknowledgments

Thanks to the Aeronautical Technological Institute (ITA), particularly the Aeronautical Systems Laboratory (LSA), for granting the necessary facilities and structure for the development of the work.

7. Contact Author Email Address

Mailing address: Praça Marechal Eduardo Gomes, 50 Vila das Acácias, 12228-900, São José dos Campos/SP - Brazil. Telephone number: +55 31 9 8833-8936. Mailto: thiagorp@ita.br.

8. Copyright Statement

References

[1] Boris A. Zárate and Juan M. Caicedo. Finite element model updating: Multiple alternatives. *Engineering Structures*, Vol. 30, 2008. ISSN 01410296. doi:10.1016/j.engstruct.2008.06.012.

[2] Castillo Zuñiga, David Fernando and Sandoval, Luiz Carlos and Barbosa, Raphaela and Maciel, Benedito and Drago, Igor. Modal Testing of a Flexible Wing UAV. *COBEM 2017*, 2018. doi:10.26678/abcm.cobem2017.cob17-2477.

[3] David F. Castillo Zuñiga and Alain Giacobini Souza and Luiz Carlos S. Goes. Development of an Aeroelastic In-Flight Testing System for a Flexible Wing Unmanned Aerial Vehicle using Acceleration and Strain Sensors. *American Institute of Aeronautics and Astronautics*, 2019. ISBN 978-1-62410-578-4. doi:10.2514/6.2019-2033.

[4] David F. Castillo Zuñiga and Alain Giacobini Souza and Luiz Carlos S. Goes. Flight dynamics modeling of a flexible unmanned aerial vehicle. *Mechanical Systems and Signal Processing(2020), 145, 106900*, 2020. doi:10.1016/j.ymssp.2020.106900.

[5] Gupta, Abhineet and Moreno, Claudia P. and Pfifer, Harald and Balas, Gary J. Updating a finite element based structural model of a small flexible aircraft. *AIAA SciTech Forum*, 2015. ISSN 9781624103438. doi:10.2514/6.2015-0903.

[6] Mottershead, J. E. and Friswell, M. I. Model updating in structural dynamics: A survey. *Journal of Sound and Vibration*, Vol. 167, No. 2, pp 347-375, 1993. ISSN 0022460X. doi:10.1006/jsvi.1993.1340.

[7] De Paula, Thiago Rosado; Fernandes, Vítor ; Sandoval Góes, Luiz Carlos ; Castillo Zuñiga, David Fernando ; Souza, Alain ; Annes da Silva, Roberto Gil. PARAMETER IDENTIFICATION BY UPDATING THE FINITE ELEMENT MODEL FOR A FLEXIBLE WING. *26th International Congress of Mechanical Engineering, 2021*, Proceedings of the 26th International Congress of Mechanical Engineering, 2021. doi:10.26678/ABCM.COBEM2021.COB2021-2033.

[8] Castillo Zuñiga, David Fernando; Sandoval Góes, Luiz Carlos; Marto, Adolfo Gomes; Annes da Silva, Roberto Gil. Aeroelastic Analysis and Comparison with in-Flight Testing of the Vector-P Unmanned Aerial Vehicle. *22nd International Congress of Mechanical Engineering (COBEM 2013), 2013, Ribeirão Preto. Proceedings 22nd International Congress of Mechanical Engineering (COBEM 2013)*, 2013.

[9] Cecrdle, Jiri. Updating of finite element model of aircraft structure according results of ground vibration test. *Proceedings of the Institution of Mechanical Engineers, Part G: Journal of Aerospace Engineering, (2016), 1348-1356, 230(7)*, 2016.